ICASSP 2025 - 2025 IEEE International Conference on Acoustics, Speech and Signal Processing (ICASSP) | 979-8-3503-6874-1/25/$31.00 ©2025 IEEE | DOI: 10.1109/ICASSP49660.2025.10888238

An Efficient Hybrid Quantum Variational Classifier With Matrix Product State

Wanqi Sun[1], Jungang Xu*[2], Chenghua Duan[1]
[1] School of Electronic, Electrical and Communication Engineering, University of Chinese Academy of Sciences, Beijing, China
[2] School of Computer Science and Technology, University of Chinese Academy of Sciences, Beijing, China
Emails: sunwanqi19@mails.ucas.ac.cn, xujg@ucas.ac.cn, cduan@ucas.ac.cn

***Abstract*—Matrix Product States have been extensively explored as a powerful tool for simulating quantum states in image classification task. However, most research has focused on classical simulations or computations involving high-dimensional unitaries, and significant challenges still exist in the practical preparation of Matrix Product States on quantum computers. This paper proposes a novel and practically feasible quantum variational algorithm based on Matrix Product States for image classification task. We design a hardware-efficient quantum circuit with several adjustable entangling operators to prepare the local tensors in Matrix Product States and integrate minimal residuals to ensure computational stability. We demonstrate that our algorithm can reduce the parameter complexity from growing exponentially with the system size to a linear scale. To validate the effectiveness of this quantum variational algorithm, we conducted experiments on the MNIST dataset, achieving accuracies of 99.95% and 95.96% for binary and ten-class classification tasks, which outperforms other related quantum algorithms. This work advances the practical application of quantum machine learning in resource-constrained environments of quantum computing.**

***Index Terms*—Variational quantum algorithm, Image classification, Matrix product states, Quantum circuit**

I. Introduction

The superposition and entanglement properties of quantum states are utilized to enhance data computation and processing capabilities. Matrix Product State (MPS), as a natural simulation of quantum spins, has been proven effective in capturing local features of quantum states. MPS possesses a one-dimensional chain structure, naturally allowing for data compression through truncation of MPS sites or bond dimensions [1]–[3], thus addressing the challenge of training large-scale quantum data in the era of noisy intermediate-scale quantum computing.

In the field of quantum machine learning, the MPSs demonstrate advantages in complex pattern recognition and decision-making processes for high-order data [4], [5]. Combined with Density Matrix Renormalization Group [6] (DMRG) methods, MPS has been trained as classifiers or predictors for various machine learning tasks [7]–[13]. Some researchers have employed MPS as a pre-training model to accelerate the training of quantum machine learning algorithms [14].

The physical preparation of MPS faces challenges in accurately translating the complex entanglement of MPS into quantum circuits and addressing errors and instabilities introduced by quantum hardware limitations. Previous research has explored encoding MPS into low-dimensional unitary matrices [15] or shallow quantum circuits [16], which require further compilation into hardware-efficient quantum gates. Recently, it has been proven that MPS can be precisely prepared on quantum circuits at the Log-Depth level [17].

To address these challenges, this paper provides an innovative algorithm for preparing MPS that focuses on improving the stability and efficiency of the algorithm and is successfully applied for image classification task. The main contributions of our work are as follows:

• *Circuit*. Design a chain-like circuit structure based on MPS to reduce the interference of long-range entanglement. Propose a hardware-efficient quantum circuit with several adjustable entangling operators to simulate the local tensors of MPS.

• *Error*. Introduce perturbation residuals during the MPS contraction process to control the propagation and accumulation of errors, thereby enhancing the stability and accuracy of the algorithm.

• *Application*. The image classification experiments on the MNIST [18] and Fashion-MNIST [19] datasets achieve accuracy rates of 99.95% and 95.96% for binary and ten-class classification on MNIST, and 99.95% and 86.83% on Fashion-MNIST, respectively.

• *Complexity*. The parameter complexity analysis is presented later in the paper, demonstrating the reduction of complexity from exponential growth with system size to a polynomial level.

Both experimental results and theoretical analysis support that our work is feasible and performs exceptionally well.

II. Method

A. Matrix Product States

The MPS efficiently describes the local entanglement of a many-body quantum system by decomposing the global tensor into a product of local tensors, with each local tensor corresponding to a subsystem. Mathematically, for a quantum many-body system containing N subsystems, its global quantum state $|\psi\rangle$ can be expressed as:

$$|\psi\rangle = \sum_{s_0,s_1,\cdots,s_{N-1}} \varphi_{s_0 s_1 \cdots s_{N-1}} \bigotimes_{n=0}^{N-1} |s_n\rangle, \tag{1}$$

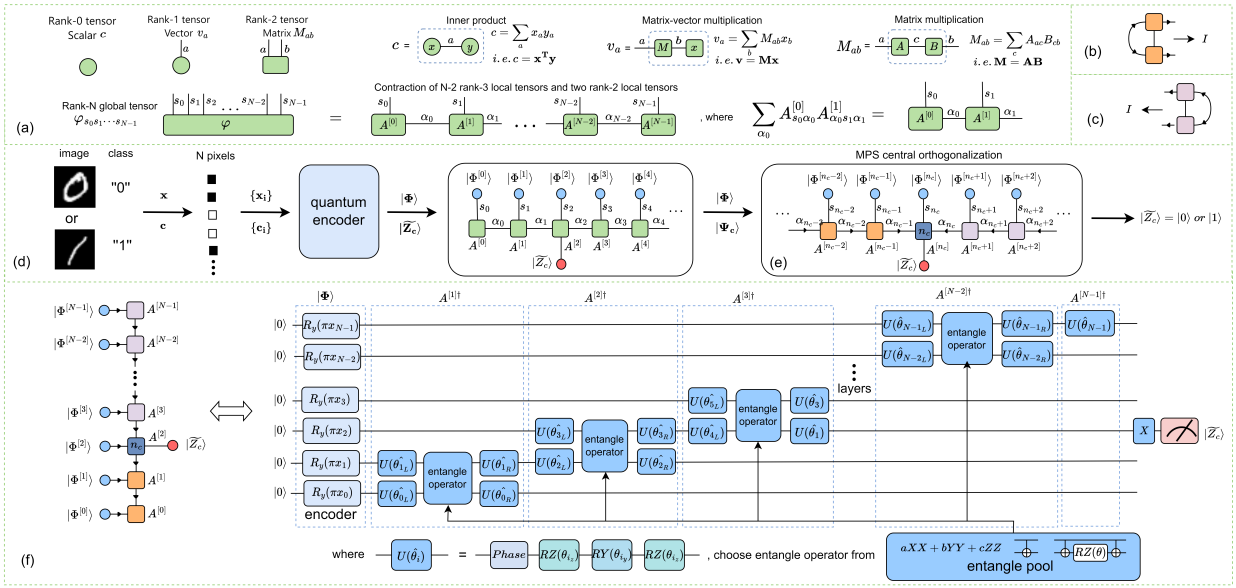

Fig. 1. Schematic Representation of MPS and the Algorithm. (a) illustrates the symbol definition of tensors and their contractions, as well as the decomposition of an rank-N tensor φ into an open boundary MPS comprising N local tensors $\{A^{[i]}\}$. Here, a shape (e.g., a square, circle, triangle) represents a tensor, and each leg corresponds to a specific index. A connecting leg between two shapes denotes tensor contraction via Einstein summation over the shared index. (b) and (c) respectively describe the isometric conditions of the tensors on the left and right sides of the orthogonal center, indicating that the corresponding tensors are isometric. (d) delineates the binary classification algorithm process: each pixel x_i of the image is encoded into a single qubit quantum state $|\Phi^{[i]}\rangle$, and the entire image is encoded as the N-qubit direct product state $|\Phi\rangle$. Each local tensor in the MPS model corresponds to the features of each pixel. During MPS training, bond-centered orthogonalization and virtual dimension truncation are performed. The central tensor's output state $|\tilde{Z}_c\rangle$ serves as the predicted class. (e) illustrates the contraction direction of the MPS in bond-centered orthogonal form, with the central tensor $A^{[n_c]}$ highlighted in blue. Tensors contract left-to-right on the left and right-to-left on the right. (f) demonstrates the mapping relationship between MPS and quantum circuits. Each local tensor $A^{[i]}$ maps to a parameterized quantum circuit composed of four single-qubit unitaries and one two-qubit unitary. Each single-qubit unitary is decomposed into rotation gates around the z and y axes, while the entangling two-qubit gate is selected from the entanglement pool.

where

$$\varphi_{s_0 s_1 \cdots s_{N-1}} = \sum_{\alpha_0, \cdots, \alpha_{N-2}} A^{[0]}_{s_0, \alpha_0} A^{[1]}_{s_1, \alpha_0, \alpha_1} \cdots A^{[N-1]}_{s_{N-1}, \alpha_{N-2}}. \tag{2}$$

The $\{|s_n\rangle\}$ denotes a set of orthonormal computational bases, and $\varphi_{s_0 s_1 \cdots s_{N-1}}$ is the complex coefficient global tensor of the quantum state, describing the superposition of different basis state combinations. As shown in Figure 1 (a), $A^{[n]}_{s_n, \alpha_{n-1}, \alpha_n}$ is the local tensor corresponding to the nth subsystem, $\{s_n\}$ denotes a set of the physical indices with dimension d, and $\{\alpha_n\}$ denotes a set of virtual indices with dimension χ. The virtual index connects the neighbor tensors, and its dimension determines the amount of entanglement that can be represented by the MPS.

B. Classification Algorithm Based on MPS

The overall procedure of the classification algorithm as shown in Figure 1 (d), which includes: (1) Encode the samples into quantum pure states; (2) Gauge the MPS model into a bond-centered orthogonal form and disentangle the quantum circuit by truncating the virtual dimensions; (3) Design quantum circuits to prepare MPS and manually adjust entangling operators from the entanglement pool, which is shown in Figure 1 (f); (4) Train the parameterized quantum circuit to obtain optimal predictions.

Quantum State Encoding. The encoding of quantum states maps each feature into vectors, mapping each sample $\{x_m\}$ into the tensor product state of multiple feature vectors, which is denoted as $|\Phi_m\rangle$:

$$|\Phi_m\rangle = \bigotimes_{n=0}^{N-1} |\phi_m^{[n]}\rangle = \bigotimes_{n=0}^{N-1} (\cos\left(\frac{\pi}{2} x_m^{[n]}\right)|0\rangle + \sin\left(\frac{\pi}{2} x_m^{[n]}\right)|1\rangle), \tag{3}$$

where the samples $\{x_m\}$ have feature dimension $d \geq 2$, $|\phi_m^{[n]}\rangle$ denotes the nth feature of the mth sample. In binary classification experiments, the category c to which a sample belongs is encoded as a single-qubit quantum state $|Z_c\rangle$. In ten-category classification experiments, one-hot encoding is used, where the dimension of c equals the number of categories K.

Central Orthogonalization. To enhance computational efficiency and stability, the next step is to gauge the MPS into the center orthogonal form as shown in Figure 1 (e).

1) Designate n_c as the orthogonal center and $A^{[n_c]}$ as the central tensor.
2) Left orthogonalization: Sequentially decompose tensors from left to right until n_c.
   - Decompose and update $A^{[n]}$ using QR or SVD: $A^{[n]}_{\alpha_{n-1} s_n \alpha_n} = \sum_\alpha A'^{[n]}_{\alpha_{n-1} s_n \alpha} M^{[n]}_{\alpha \alpha_n}$.
   - Update $A^{[n+1]}$ by contracting $M^{[n]}$: $A^{[n+1]}_{\alpha s_{n+1} \alpha_{n+1}} \leftarrow \sum_{\alpha_n} M^{[n]}_{\alpha \alpha_n} A^{[n+1]}_{\alpha_n s_{n+1} \alpha_{n+1}}$.
3) Right orthogonalization: Sequentially decompose tensors from right to left until n_c.
   - Decompose and update $A^{[n]}$ using QR or SVD: $A^{[n]}_{\alpha_{n-1} s_n \alpha_n} = \sum_\alpha M^{[n]}_{\alpha_{n-1} \alpha} A'^{[n]}_{\alpha s_n \alpha_n}$.

- Update $A^{[n-1]}$ by contracting $M^{[n]}$: $A^{[n-1]}_{\alpha_{n-2}s_{n-1}\alpha} \leftarrow \sum_{\alpha_{n-1}} A^{[n-1]}_{\alpha_{n-2}s_{n-1}\alpha_{n-1}} M^{[n-1]}_{\alpha_{n-1}\alpha}$.

The above decomposition-contraction process is equivalent to inserting $M^{[n]}(M^{[n]})^{-1} = I$ on the virtual index α_n, which constitutes a gauge transformation and does not change the quantum state represented by the MPS. At this point, the local tensors of the MPS satisfy the orthogonal constraints as shown in Figure 1 (b) and Figure 1 (c).

Optimal Truncation of Virtual Dimension. Next, the virtual dimension of the MPS is truncated to a smaller χ. Since the virtual dimension χ controls the degree of local entanglement, this truncation step can reduce redundant entanglement in the MPS quantum circuit. According to the relationship between Schmidt decomposition and singular value decomposition, the bipartite entanglement entropy of the MPS corresponds to the singular spectrum of the central matrix $M^{[n_c]}$. Therefore, we perform the truncation of the virtual dimension by conducting a singular value decomposition on the central matrix. Set $n_c = 0$, the main steps of the virtual dimension truncation are as follows:

1) Perform SVD on the central matrix: $M^{[n_c]}_{\alpha_{n_c}\alpha'_{n_c}} = \sum_{\alpha\alpha'} U_{\alpha_{n_c}\alpha}\Gamma_{\alpha\alpha'}V_{\alpha'_{n_c}\alpha'}$.
2) Retain the first χ' singular values and the corresponding singular vectors, and contract transformation matrix $U_{\alpha_{n_c}\alpha}$ into the n_cth local tensor: $A^{[n_c]}_{\alpha_{n_c-1}s_{n_c}\alpha} \leftarrow \sum_{\alpha_{n_c}} A^{[n_c]}_{\alpha_{n_c-1}s_{n_c}\alpha}U_{\alpha_{n_c}\alpha}$.
3) Update the local tensor at n_c+1: $A^{[n_c+1]}_{\alpha s_{n_c}\alpha_{n_c+1}} \leftarrow \sum_{\alpha_{n_c}} V^*_{\alpha_{n_c}\alpha}A^{[n_c+1]}_{\alpha_{n_c}s_{n_c}\alpha_{n_c+1}}$.
4) Update the orthogonal center $n_c \leftarrow n_c+1$ and repeat steps 1) – 3) until $n_c = N-1$.

Similar to the DMRG method, we move the orthogonal center from the far left to the far right and then back from the far right to the far left, thus updating each local tensor in the MPS twice. Such a full left-to-right and then right-to-left update cycle is termed as one sweep. In our experiments, the number of sweeps is set to 10.

Introduce the Residual Terms. When the MPS with a chain structure becomes excessively lengthy, the accumulation of computational errors from multiple products may lead to an "orthogonality catastrophe". To ensure computational stability, in addition to maintaining orthogonality of the MPS, truncating bond dimensions and regular normalization of the MPS, we introduce a small residual term ϵ during the contraction of local tensors [20]. This approach ensures that the magnitude of the contraction varies linearly with the number of contracted tensors, rather than exponentially. The details are as follows:

1) The MPS contracts from both ends towards the orthogonal center: $\sum_{\alpha_n,s_n} v^{[n]}_{\alpha_n}\phi^{[n]}_{s_n}A^{[n]}_{\alpha_n s_n\alpha_{n+1}} = v^{[n+1]}_{\alpha_{n+1}}$, where the boundary tensors are $v^{[0]} = [1]$ and $v^{[N-1]} = [1]$.
2) The local tensors with residual terms satisfy: $A^{[n]}_{:,0,:} = I, |A^{[n]}_{:,1,:}| \sim \epsilon$.
3) Based on 1) and 2), we can obtain:
$$\begin{aligned}|v^{[n]}| &= |v^{[n-1]} + x_{n-1}v^{[n-1]}A^{[n-1]}_{:,1,:}| \\ &\le (1+|x_{n-1}|\epsilon)|v^{[n-1]}| \\ &\le (1+|x_{n-1}|\epsilon)(1+|x_{n-2}|\epsilon)|v^{[n-2]}| \\ &\lesssim [1+(|x_{n-1}|+|x_{n-2}|)\epsilon]|v^{[n-2]}| \\ &\lesssim [1+K\bar{x}\epsilon]\big|v^{[n-K]}\big|,\end{aligned}$$
where K is a constant.

Thus, during the update process, the magnitude of environment tensor $v^{[n]}$ approximately varies linearly with the number of contracted tensors K, rather than growing exponentially.

Design Circuit to Prepare the MPS. Our design of quantum circuit for preparing MPS is inspired by the concept of disentangling operator. Consider a complex quantum state $|\psi\rangle$, which is transformed into a simpler state (such as the standard basis state $|0\rangle$) by applying a disentangling operator $\mathcal{U}$, i.e., $\mathcal{U}|\psi\rangle = |0\rangle$. Subsequently, the complex state $|\psi\rangle$ can be reconstructed from the basis state $|0\rangle$ by applying the conjugate transpose $\mathcal{U}^\dagger$, i.e., $|\psi\rangle = \mathcal{U}^\dagger\mathcal{U}|\psi\rangle = \mathcal{U}^\dagger|0\rangle$.

The local tensor $A^{[n]}$ is simulated using a parameterized quantum circuit $\mathcal{U}^{[n]\dagger}$. In constructing the quantum state $|\psi\rangle$, the unitary transformations $\mathcal{U}^{[n]\dagger}$ are sequentially applied to the initial state $|\psi_{\text{init}}\rangle = \bigotimes_{n=0}^{N-1}|s_n\rangle$. This approach progressively introduces entanglement and local transformations, ensuring that the state $|\psi\rangle$ is constructed accurately. Combining Eq. (1) and (2), it can be deduced that state $|\psi\rangle$ satisfies:
$$\begin{aligned}|\psi\rangle &= \sum_{\alpha_0,\cdots,\alpha_{N-2}} A^{[0]}_{s_0,\alpha_0}A^{[1]}_{s_1,\alpha_0,\alpha_1}\cdots A^{[N-1]}_{s_{N-1},\alpha_{N-2}}\bigotimes_{n=0}^{N-1}|s_n\rangle \\ &= \mathcal{U}^{[0]\dagger}\mathcal{U}^{[1]\dagger}\cdots\mathcal{U}^{[N-1]\dagger}|\psi_{\text{init}}\rangle \\ &= \mathcal{U}^\dagger|\psi_{\text{init}}\rangle.\end{aligned} \tag{4}$$
Given that all quantum logic gates employed are unitary, it can be easily demonstrated that the unitary $\mathcal{U}^{[n]\dagger}$ adheres to the aforementioned orthogonality property. When the MPS subsystem is spanned by two qubits, according to the Cartan decomposition, the construction of $\mathcal{U}^{[n]\dagger}$ can be expressed as:
$$\mathcal{U}^{[n]\dagger} = (U(\hat{\theta}_{n_L})\otimes U(\hat{\theta}_{n+1_L}))\mathcal{O}_e^{[n]}(U(\hat{\theta}_{n_R})\otimes U(\hat{\theta}_{n+1_R})), \tag{5}$$
where $\mathcal{O}_e^{[n]}$ denotes the entangle operator, and $\mathcal{O}_e^{[n]}$ is chosen from the entangle pool $\{CNOT, CRZ, \alpha_x XX + \alpha_y YY + \alpha_z ZZ\}$, representing the entanglement between qubits. $U(\hat{\theta}_{n_L})$, $U(\hat{\theta}_{n+1_L})$, $U(\hat{\theta}_{n_R})$, and $U(\hat{\theta}_{n+1_R})$ are single-qubit unitary operations acting on the nth subsystem, which can be decomposed into parameterized rotation gates according to the Solovay-Kitaev (SK) theorem:
$$U(\hat{\theta_n}) = e^{i\theta_{n_p}}RZ(\theta_{n_z})RY(\theta_{n_y})RZ(\theta_{n_z}). \tag{6}$$
Then, the appropriate objective function is selected according to the task scenario, and an optimization algorithm such as Adam is used to adjust the quantum gate parameters to minimize the loss between the output and the target.

Objective Function. For the mth training sample x_m, we define the mapping function f to perform the classification

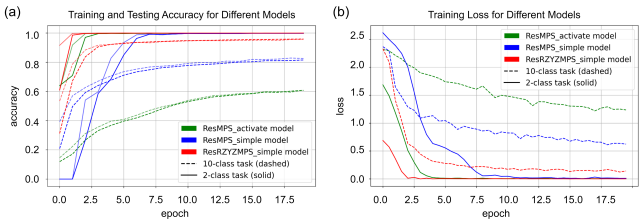

Fig. 2. Experimental Results. (a) compares accuracy, and (b) compares loss for MPS-based models on binary and ten-class tasks. Dark shades represent training data, light shades represent testing data, with the same color for each model.

TABLE I
ACCURACY OF DIFFERENT MODELS ON IMAGE CLASSIFICATION TASKS WITH THE MNIST AND FASHION-MNIST DATASETS.

Model	MNIST			Fashion-MNIST		
	10 class	4 class	2 class	10 class	4 class	2 class
MPS [20]	88.14	96.65	99.81	79.98	91.45	99.81
MPScircuit	**95.96**	**97.59**	**99.95**	**86.83**	**94.25**	**99.95**
ReLUMPS	69.87	86.90	99.39	69.02	66.80	96.65
QNCA [22]	77.50	-	-	-	-	-
QTL [23]	94.51	-	-	-	-	-
EQFE-CNN [24]	93.18	96.90	-	85.27	-	97.84
HQLSTM [25]	-	-	99.15	-	-	-
QCNN [26]	-	-	97.62	-	-	-
VQcirciut [27]	-	-	-	80.20	-	-

task as follows:

$$Z_c^{[m]} = f(x_m;\boldsymbol{\varphi}) = \sum_{s_0,\cdots,s_{N-1}} \varphi_{cs_0,\cdots,s_{N-1}} x_m^{[0]} x_m^{[1]} \cdots x_m^{[\mathrm{N}-1]}, \quad (7)$$

where $\boldsymbol{\varphi}$ denotes the parameterized variational quantum circuit; $Z_c^{[m]}$ is a K-dimensional vector that performs one-hot encoding of the category, representing the output corresponding to the sample x_m. By calculating the distance between $Z_c^{[m]}$ and the label vector, the label corresponding to the minimum distance is the predicted label of the sample x_m. This process essentially defines a simple machine learning model parameterized by the MPS variational quantum circuit $\boldsymbol{\varphi}$. The loss function is defined as:

$$L = \frac{1}{M}\sum_{m=0}^{M-1}\left|Z_c^{[m]} - \widetilde{Z}^{[m]}\right|^2, \quad (8)$$

where M is the total number of training samples, and $\widetilde{Z}^{[m]}$ is the label vector corresponding to the correct label of x_m. The label index is positioned at the central tensor and moves together with the orthogonal center. The update formula for the nth local circuit is shown below:

$$\mathcal{U}^{[n]\dagger} \leftarrow \mathcal{U}^{[n]\dagger} - \eta\frac{\partial L}{\partial \mathcal{U}^{[n]\dagger}}, \quad (9)$$

where the gradient term satisfies:

$$\frac{\partial L}{\partial \mathcal{U}^{[n]\dagger}} = 2\mathcal{U}^{[n]\dagger} - \frac{2}{M}\sum_{m=0}^{M-1}\frac{1}{\langle\psi|\tilde{Z}^{[m]}|\Phi_m\rangle}\frac{\partial\langle\psi|\tilde{Z}^{[m]}|\Phi_m\rangle}{\mathcal{U}^{[n]\dagger}}. \quad (10)$$

During this process, normalization is manually performed to ensure that the central tensor satisfies the normalization condition $|\mathcal{U}^{[n]}| = 1$, i.e., $\frac{2\mathcal{U}^{[n]}}{|\mathcal{U}^{[n]}|^2} = 2\mathcal{U}^{[n]}$.

III. Results and Analysis

All experiments were conducted with the high-performance library PyTorch [21] on both the MNIST and Fashion-MNIST datasets. Both datasets consist of 60,000 training images and 10,000 testing images, and each image is a 28×28 grayscale image. MNIST contains handwritten digit images from '0' to '9', while Fashion-MNIST consists of 10 classes of clothing items and accessories, such as shirts, shoes, and bags.

Experimental Results. Our experimental results are displayed in Figure 2, and comparative results are in Table I. For the classification task, our algorithm converges faster and performs better than the standard MPS numerical method and the MPS with ReLU activation layer. It is found that the results of the MPS with ReLU activation layer are very unstable, and only a few cases can reach the results close to the standard MPS. The accuracy in most cases is as shown in Figure 2, which may be due to its nonlinear activation layer. This validates that our algorithm captures key features more efficiently and accurately, and the model outperforms traditional MPS methods on the test dataset.

Complexity Analysis. In this paper, each physical dimension of the MPS is equal to the virtual dimension, i.e., $d = \chi$. The number of parameters for the rank-2 tensors at the ends of the MPS is $\chi d = d^2$, and for the $(N-2)$ rank-3 tensors in the middle, the number of parameters is $\chi^2 d = d^3$. The parameter complexity of the MPS satisfies $2d\chi + (N-2)d\chi^2 \approx \mathcal{O}(Nd^3)$, indicating that the complexity of MPS parameters is linearly related to the number of subsystems N. In a Hilbert space spanned by $N\log_2 d$ qubits, the global parameter complexity of the quantum state is $2^N d$, which is exponentially related to N, with $Nd^3 \ll 2^N d$. If the subsystem size is considered as a constant, then MPS circuit simulation effectively reduces the parameter complexity of the global state from exponential to linear scale.

IV. Conclusion and Discussion

The proposed hybrid quantum variational strategy for classification task fully leverages the structural advantages of MPS, providing a circuit design protocol for preparing MPS on quantum computers. It is proved that our algorithm not only can reduce the parameter complexity from exponential to linear growth with respect to the number of qubits, but also can prevent the gradient explosion by introducing residual terms to control errors. Experimental results show that the proposed classifier achieves higher accuracy than other MPS algorithms with the same settings and relevant quantum classifiers, and it also converges faster. Additionally, our work provides a new perspective and strategy for preparing complex many-body states on quantum computers.

Theoretically, MPS's chain structure has strong short-range correlations, resulting in better performance in sequential tasks. Considering the diverse applications of classifiers, further exploration in circuit architecture design is essential. Limited by current quantum hardware, noise mitigation and error correction techniques can be introduced to enhance the algorithm's practical performance.

REFERENCES

[1] S.-H. Lin, R. Dilip, A. G. Green, A. Smith, and F. Pollmann, "Real- and imaginary-time evolution with compressed quantum circuits," *PRX Quantum*, vol. 2, p. 010342, 2021.

[2] J. A. Bengua, P. N. Ho, H. D. Tuan, and M. N. Do, "Matrix product state for higher-order tensor compression and classification," *IEEE Transactions on Signal Processing*, vol. 65, pp. 4019–4030, 2017.

[3] D. E. Parker, X. Cao, and M. P. Zaletel, "Local matrix product operators: Canonical form, compression, and control theory," *Physical Review B*, vol. 102, p. 035147, 2020.

[4] Z.-Y. Han, J. Wang, H. Fan, L. Wang, and P. Zhang, "Unsupervised generative modeling using matrix product states," *Physical Review X*, vol. 8, p. 031012, 2018.

[5] L.-H. Gong, L.-Z. Xiang, S.-H. Liu, and N.-R. Zhou, "Born machine model based on matrix product state quantum circuit," *Physica A: Statistical Mechanics and its Applications*, vol. 593, p. 126907, 2022.

[6] U. Schollwöck, "The density-matrix renormalization group," *Reviews of modern physics*, vol. 77, pp. 259–315, 2005.

[7] J. Carrasquilla, "Machine learning for quantum matter," *Advances in Physics: X*, vol. 5, p. 1797528, 2020.

[8] M. Schuld, "Supervised quantum machine learning models are kernel methods (2021)," *arXiv preprint arXiv:2101.11020*, 2023.

[9] X. Shi, Y. Shang, and C. Guo, "Clustering using matrix product states," *Physical Review A*, vol. 105, p. 052424, 2022.

[10] B. Žunkovič, "Deep tensor networks with matrix product operators," *Quantum Machine Intelligence*, vol. 4, p. 21, 2022.

[11] H.-Y. Huang, R. Kueng, G. Torlai, V. V. Albert, and J. Preskill, "Provably efficient machine learning for quantum many-body problems," *Science*, vol. 377, p. eabk3333, 2022.

[12] A. Mossi, B. Žunkovic, and K. Flouris, "A matrix product state model for simultaneous classification and generation," *arXiv preprint arXiv:2406.17441*, 2024.

[13] K. C. Smith, A. Khan, B. K. Clark, S. Girvin, and T.-C. Wei, "Constant-depth preparation of matrix product states with adaptive quantum circuits," *PRX Quantum*, vol. 5, p. 030344, 2024.

[14] J. Dborin, F. Barratt, V. Wimalaweera, L. Wright, and A. G. Green, "Matrix product state pre-training for quantum machine learning," *Quantum Science and Technology*, vol. 7, p. 035014, 2022.

[15] S.-J. Ran, "Encoding of matrix product states into quantum circuits of one-and two-qubit gates," *Physical Review A*, vol. 101, p. 032310, 2020.

[16] M. S. Rudolph, J. Chen, J. Miller, A. Acharya, and A. Perdomo-Ortiz, "Decomposition of matrix product states into shallow quantum circuits," *Quantum Science and Technology*, vol. 9, p. 015012, 2023.

[17] D. Malz, G. Styliaris, Z.-Y. Wei, and J. I. Cirac, "Preparation of matrix product states with log-depth quantum circuits," *Physical Review Letters*, vol. 132, p. 040404, 2024.

[18] Y. LeCun, L. Bottou, Y. Bengio, and P. Haffner, "Gradient-based learning applied to document recognition," *Proceedings of the IEEE*, vol. 86, pp. 2278–2324, 1998.

[19] H. Xiao, K. Rasul, and R. Vollgraf, "Fashion-mnist: a novel image dataset for benchmarking machine learning algorithms," *arXiv preprint arXiv:1708.07747*, 2017.

[20] Y.-M. Meng, J. Zhang, P. Zhang, C. Gao, and S.-J. Ran, "Residual matrix product state for machine learning," *SciPost Physics*, vol. 14, p. 142, 2023.

[21] A. Paszke, S. Gross, F. Massa, A. Lerer, J. Bradbury, G. Chanan, T. Killeen, Z. Lin, N. Gimelshein, L. Antiga *et al.*, "Pytorch: An imperative style, high-performance deep learning library," *Advances in neural information processing systems*, vol. 32, 2019.

[22] S. Johri, S. Debnath, A. Mocherla, A. Singk, A. Prakash, J. Kim, and I. Kerenidis, "Nearest centroid classification on a trapped ion quantum computer," *npj Quantum Information*, vol. 7, p. 122, 2021.

[23] S. Sarkar, "Quantum transfer learning for mnist classification using a hybrid quantum-classical approach," *arXiv preprint arXiv:2408.03351*, 2024.

[24] T. Dou, G. Zhang, and W. Cui, "Efficient quantum feature extraction for cnn-based learning," *Journal of the Franklin Institute*, vol. 360, pp. 7438–7456, 2023.

[25] G. Yang, S. Chao, M. Nie *et al.*, "Construction method of hybrid quantum long-short term memory neural network for image classification," *Acta Physica Sinica*, vol. 72, pp. 474–487, 2023.

[26] I. Cong, S. Choi, and M. D. Lukin, "Quantum convolutional neural networks," *Nature Physics*, vol. 15, pp. 1273–1278, 2019.

[27] K. Shen, B. Jobst, E. Shishenina, and F. Pollmann, "Classification of the fashion-mnist dataset on a quantum computer," *arXiv preprint arXiv:2403.02405*, 2024.